

1 **Contrasting spatial and seasonal trends of methylmercury exposure**
2 **pathways of Arctic seabirds: combination of large-scale tracking and**
3 **stable isotopic approaches**

4
5 Marina Renedo^{1,2,*}, David Amouroux², Céline Albert¹, Sylvain Bérail², Vegard S.
6 Bråthen³, Maria Gavrilov⁴, David Grémillet^{5,6}, Hálfór H. Helgason⁷, Dariusz Jakubas⁸,
7 Anders Mosbech⁹, Hallvard Strøm⁷, Emmanuel Tessier², Katarzyna Wojczulanis-
8 Jakubas⁸, Paco Bustamante^{1,10}, Jérôme Fort^{1*}

9 ¹ Littoral Environnement et Sociétés (LIENSs), UMR 7266 CNRS- La Rochelle Université, 2 rue Olympe de Gouges,
10 17000 La Rochelle, France

11 ² Université de Pau et des Pays de l'Adour, E2S UPPA, CNRS, IPREM, Institut des Sciences Analytiques et de Physico-
12 chimie pour l'Environnement et les matériaux, Pau, France

13 ³ Norwegian Institute for Nature Research, Trondheim, Norway

14 ⁴ Arctic and Antarctic Research Institute, 38 Bering Street, 199397, Saint-Petersburg, Russia

15 ⁵ Centre d'Etudes Biologiques de Chizé, UMR 7372 CNRS –La Rochelle Université, 405 Route de Prissé la Charrière
16 79360 Villiers-en-Bois, France

17 ⁶ Percy FitzPatrick Institute, DST/NRF Centre of Excellence, University of Cape Town, Rondebosch, South Africa

18 ⁷ Norwegian Polar Institute, Tromsø, Norway

19 ⁸ Gdańsk University, Faculty of Biology, Gdańsk, Poland

20 ⁹ Aarhus University, Department of Bioscience, Roskilde, Denmark

21 ¹⁰ Institut Universitaire de France (IUF), 1 rue Descartes, 75005 Paris, France

22
23 **Corresponding authors: marina.renedo@ird.fr, jerome.fort@univ-lr.fr*

24

25

26

27

28

29 **Abstract**

30 Despite the limited direct anthropogenic mercury (Hg) inputs in the circumpolar Arctic,
31 elevated concentrations of methylmercury (MeHg) are accumulated in Arctic marine
32 biota. However, the MeHg production and bioaccumulation pathways in these ecosystems
33 are not completely unravelled. We measured Hg concentrations and stable isotope ratios
34 of Hg, carbon and nitrogen in feathers and blood of geolocator-tracked little auk *Alle alle*
35 from five Arctic breeding colonies. The wide-range spatial mobility and tissue-specific
36 Hg integration times of this planktivorous seabird allowed the exploration of their spatial
37 (wintering quarters/breeding grounds) and seasonal (non-breeding/breeding periods)
38 MeHg exposure. An east-to-west increase of head feather Hg concentrations (1.74-3.48
39 $\mu\text{g}\cdot\text{g}^{-1}$) was accompanied by significant spatial trends of Hg isotope (particularly $\Delta^{199}\text{Hg}$:
40 0.96 to 1.13‰) and carbon isotope ($\delta^{13}\text{C}$: -20.6 to -19.4‰) ratios. These trends suggest
41 distinct mixing/proportion of MeHg sources between western North Atlantic and eastern
42 Arctic regions. Higher $\Delta^{199}\text{Hg}$ values (+0.4‰) in northern colonies indicate an
43 accumulation of more photochemically impacted MeHg, supporting shallow MeHg
44 production and bioaccumulation in High Arctic waters. The combination of seabird tissue
45 isotopic analysis and spatial-tracking helps tracing the MeHg sources at various spatio-
46 temporal scales.

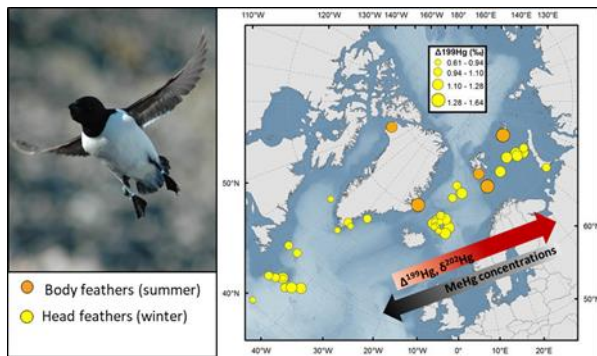
47

48

49

50

51 TOCArt- graphical abstract



52

53

54 1 Introduction

55 Mercury (Hg) induces major risks for wildlife and human health, especially under its
56 methylated form (methylmercury, MeHg), a potent bioaccumulative neurotoxin ¹, which
57 is mainly assimilated via fish and seafood consumption. In the ocean, MeHg production
58 mainly occurs by biotic *in situ* methylation of inorganic Hg ^{2,3}. Once formed, MeHg
59 incorporates into the food webs and biomagnifies its concentrations leading to life-
60 impacting levels in top predators and humans. Despite little direct anthropogenic pressure
61 in the Arctic region, Arctic ecosystems are subject to contamination by Hg transported
62 from lower latitudes. Indeed, total Hg concentrations measured in the Arctic surface
63 seawater are up to 2-fold higher compared to other oceanic regions ^{4,5}. Sea-ice melting,
64 direct atmospheric deposition and continental inputs originating from soil erosion and
65 riverine circulation are considered major drivers of the high Hg levels in the Arctic ⁶⁻¹⁰.
66 However, the MeHg production pathways and zones in the Arctic Ocean are still not
67 completely identified. Several studies demonstrated that Hg in Arctic marine
68 environments may be methylated in the water column or sediments ^{2,11}. Potential Hg
69 methylating bacteria were also identified in Antarctic sea ice ¹². Recent findings and

70 modelling studies evidenced that the largest net MeHg production in Arctic water
71 columns may occur in oxic waters at the subsurface layer (20–200 m) ^{6,13}. A new study
72 also reported the high abundance of Hg methylating gens in the oxic subsurface waters
73 of the global ocean ¹⁴, where the highest MeHg concentrations are typically observed ⁴.
74 All these findings suggest that Hg methylation in oxic waters could be a significant source
75 of MeHg towards Arctic marine food webs. Although policy implementations for the
76 reduction of anthropogenic Hg emissions were achieved over the last 30 years in some
77 parts of the world, Hg levels continue to increase in biota from several regions of the
78 Arctic ¹⁵. Medium to high predators such as seabirds are exposed to significant
79 environmental MeHg concentrations through their diet ^{15,16} and have been extensively
80 studied as bioindicators of Hg exposure in marine food webs (e.g ^{17,18}), including the
81 Arctic ^{19–21}. Specific foraging habitats and migratory movements of Arctic seabirds
82 strongly determine their exposure to distinct environmental MeHg sources in marine
83 ecosystems ^{22,23}. However, studies on Hg exposure in Arctic seabirds have commonly put
84 the focus towards the breeding season (summer) when seabirds are more accessible for
85 researchers. Consequently, the investigation of Hg exposure during the non-breeding
86 season is still scarce due to sampling logistical difficulties.

87 The combination of carbon and nitrogen stable isotopes with Hg stable isotopes has
88 demonstrated its suitability for the identification of Hg sources and the associated
89 geochemical processes in the different marine compartments ^{24–26}. Therefore, its use can
90 help understanding Hg exposure pathways of seabirds according to their migratory
91 behaviour. Hg has seven stable isotopes (196 to 204) and fractionates dependently and
92 independently of the isotopic masses. The combined use of Hg isotopic mass-dependent
93 (MDF, e.g. $\delta^{202}\text{Hg}$) and mass-independent (MIF, e.g. $\Delta^{199}\text{Hg}$) fractionation enables the

94 quantification of processes and the identification of sources and pathways of Hg in the
95 environment²⁷, including marine ecosystems^{25,26,28,29}. MDF of Hg isotopes occurs during
96 many physical, chemical or biological processes^{30–33}. However, large Hg MIF of odd
97 isotopes ($\Delta^{199}\text{Hg}$ and $\Delta^{201}\text{Hg}$) is observed during light-induced reactions, such as
98 inorganic Hg photoreduction and MeHg photodemethylation. Hg MIF signature is not
99 affected by biological or trophic processes, so it is preserved up to the food webs³⁴, then
100 presenting a significant advantage to trace Hg marine sources. For instance, Arctic marine
101 top predators reported much higher Hg odd MIF values (more photochemically impacted
102 Hg) in non-ice covered regions, relating the importance of the accelerated melting of sea
103 ice on the Hg polar cycle^{25,35}. Also, consistent decrease of Hg odd MIF (and MDF) in
104 pelagic fish according to their foraging depth in the North Pacific Ocean demonstrated
105 the dilution of surface MeHg by *in situ* methylated Hg at depth³. More recently
106 discovered, Hg MIF of even Hg isotopes (reported as $\Delta^{200}\text{Hg}$) seems to occur during
107 complex atmospheric mechanisms such as photo-oxidation in the tropopause³⁶. Even-
108 MIF is not induced during any biogeochemical nor photochemical processes in the lower
109 troposphere or the photic zone^{36–38}, therefore the signature is preserved and useful to
110 identify major potential Hg sources of atmospheric origin^{10,39,40}. Due to the different
111 combinations of the processes involving Hg transformations in the environment, Hg
112 isotopes fractionate differently and with different degrees of magnitude in every specific
113 environmental compartment. Thus, the analysis of Hg stable isotopes of mobile predators
114 such as Arctic seabirds can give access to interesting information about MeHg trophic
115 sources at large scales of the Arctic Ocean and neighbouring water bodies.

116 Here we propose an original approach consisting in the combination of isotopic analyses
117 (Hg, C and N) and wildlife tracking to provide new information about MeHg exposure

118 pathways of seabirds at both temporal and spatial scales. For this purpose, we focused on
119 the little auk (or dovekie, *Alle alle*), the most numerous seabird species breeding in the
120 High Arctic (between 37 to 40 million breeding pairs estimated ^{41,42}). Little auks have
121 several ecological advantages for their use as a bioindicator models. 1) They are
122 zooplanktivorous and mainly feed on copepods belonging to two *Calanus* species (i.e.,
123 *C. glacialis* and *C. hyperboreus*) during the breeding period ⁴³. Therefore, they reflect
124 MeHg accumulation in a short food chain that is strongly dependent on sea ice abundance
125 and seawater temperature ⁴⁴. 2) They exhibit colony specific wintering areas ⁴⁵, then
126 reflecting wide-ranging spatial variability of Hg exposure ⁴⁶. 3) Little auks moult their
127 feathers twice during their annual cycle: a partial moult (head, neck and throat feathers,
128 hereafter ‘head feathers’) during the pre-breeding period (in ca. April) and a complete
129 post-breeding moult in September ¹³. During moult, seabirds excrete the Hg accumulated
130 in their body tissues into feathers ⁴⁷. Thus, feather Hg reflects blood Hg levels at the time
131 of feather growth which occurred at the last moulting sequence ⁴⁸, then integrating Hg
132 from current diet and/or the remobilization of Hg from tissues during moult. Thereby, the
133 different Hg integration times between the types of feathers allow studying Hg exposure
134 during both the non-breeding (head feathers) and the breeding (body feathers) periods in
135 a same individual ⁴⁶. Besides, C and N isotopic ratios of blood sampled during the
136 breeding – chick rearing – period can provide information about summer diet and then be
137 compared to Hg levels and isotopic composition in body feathers of little auks ^{49,50}. We
138 hypothesized that variations of tissue-specific Hg isotopic signatures (body vs head
139 feathers) will allow reflecting the seasonal variability (summer vs winter) on the Hg
140 cycling. Besides, the exploration of both spatial grounds and isotopic information (Hg, C

141 and N) would help tracking distinct sources of Hg contamination along with seabird
142 migratory circulation.

143 **2 Material and methods**

144 2.1 Sampling sites and description of sample collection

145 This study was conducted during the seabird breeding seasons of 2015 and 2016 at five
146 colonies of the Arctic Ocean: Franz Josef Land (FJL) (Hooker Island; 80.23°N, 53.01°
147 E), Bear Island (Bjørnøya; 74.45°N, 19.04° E), East Greenland (Kap Høegh; 70.72°N,
148 21.55°W), Spitsbergen (Hornsund; 76.97°N, 15.78 °E) and North West Greenland
149 (Thule; 77.47°N, 69.22° W). Blood and feathers were sampled from ten individuals per
150 colony (n=50 for the 5 colonies). Individuals from all sites, but Thule, were equipped with
151 a miniature geolocator data-logger (GLS, Biotrack MK4083 or Migrate Technology C65)
152 to track their non-breeding movements and distribution, as described in previous works
153 ^{45,51,52}. We treated GLS tracking data from 1st December to 30th January (period when all
154 little auks were at their winter grounds) and calculated the median individual winter
155 latitude and longitude for each individual separately.

156 2.2 Description of analytical methods

157 **Sample preparation, analyses of total Hg and Hg species concentrations**

158 Body and head feathers were cleaned in a 2:1 chloroform:methanol solution for 5 min in
159 an ultrasonic bath, followed by two methanol rinses to remove surface impurities, and
160 then oven dried at 50 °C during 48 h and homogenized to powder ⁴⁶. Since fluctuations
161 of Hg concentrations have been observed among and within individual feathers from the
162 same bird ^{53,54}, we pooled a representative number of feathers of each individual (5-8

163 feathers) to limit the variability and provide results as accurately as possible. Blood
164 samples were dried, lyophilized and ground to powder as described in a previous work ⁴⁶.
165 Feather and blood total Hg concentration (hereafter expressed as $\mu\text{g}\cdot\text{g}^{-1}$, dry weight) was
166 quantified by using an advanced Hg analyser (AMA-254, Altec).

167 Prior to Hg speciation analyses, blood and feathers (0.01–0.05 g) were digested following
168 a previously developed method by microwave-assisted extraction (using a Discover SP-
169 D microwave, CEM Corporation) ^{55,56}. We used 5 mL of tetramethylammonium
170 hydroxide (25% TMAH in H₂O, Sigma Aldrich) for blood samples and 5 mL nitric acid
171 (HNO₃·6N, INSTRA quality) for feather Hg extraction. The extraction was carried out
172 in CEM Pyrex vessels by 1 min of warming up to 75 °C and 3 min at 75 °C with magnetic
173 agitation to homogenise the samples. Quantification of Hg species was carried out by
174 isotope dilution analysis (details in ⁵⁵), using a GC-ICP-MS Trace Ultra GC equipped
175 with a Triplus RSH autosampler coupled to an ICP-MS XSeries II (Thermo Scientific,
176 USA). We performed Hg speciation analyses of certified reference materials (CRM) for
177 QA/QC purposes ([Table S1](#)). Human hair reference material (NIES-13) and feather
178 internal reference material (F-KP, king penguin feathers) were used for validation of
179 feather analyses (keratin-based matrixes). Blood analyses were validated with dogfish
180 liver reference material (Dolt-5) and with internal reference material (RBC-KP, king
181 penguins red blood cells). The reported results total Hg concentrations obtained by Hg
182 speciation analyses (i.e., the sum of inorganic and organic Hg) were compared to total Hg
183 concentrations obtained by AMA-254 to verify the recovery of the extraction. Recoveries
184 of Hg and MeHg concentrations with respect to the reference values for each material
185 varied between 92 and 108% ([Table S1](#)).

186 **Total Hg isotope analyses**

187 Feather (and blood) samples (0.05–0.10 g) were digested with 3 or 5 mL of HNO₃ acid
188 (65%, INSTRA quality) after a predigestion step overnight at room temperature. Hg
189 extraction was carried out by Hotblock heating at 75 °C during 8 h (6 h in HNO₃ and 2 h
190 more after addition of 1/3 of the total volume of H₂O₂ 30%, ULTREX quality). The digest
191 mixtures were finally diluted in an acidic matrix (10% HNO₃ and 2% HCl) with final Hg
192 concentrations ranging from 0.5 to 1 ng·mL⁻¹. Hg isotopic composition was determined
193 using cold-vapor generator (CVG)-MC-ICPMS (Nu Instruments), detailed in previous
194 work ⁵⁶. Hg isotopic values were reported as delta notation, calculated relative to the
195 bracketing standard NIST SRM-3133 reference material to allow interlaboratory
196 comparisons, as described in the SI. NIST SRM-997 thallium standard solution was used
197 for the instrumental mass-bias correction using the exponential law. Secondary standard
198 NIST RM-8160 (previously UM-Almadén standard) was used for validation of the
199 analytical session (Table S2).

200 Recoveries of extraction were verified for all samples by checking the signal intensity
201 obtained on the MC-ICPMS for diluted extracts relative to NIST 3133 standard (with an
202 approximate uncertainty of ±15%). Total Hg concentrations in the extract solution were
203 compared to the concentrations found by AMA-254 analyses to assess method recovery.
204 Total Hg concentrations in the extract solution were compared to the concentrations found
205 by AMA-254 analyses to assess method recovery. Average recoveries obtained were 98
206 ± 14% for feathers (n = 104) and 100 ± 2% for blood samples (n = 102). Accuracy of Hg
207 isotopic analyses for keratin matrixes was evaluated with validated human hair material
208 NIES-13 isotopic composition ⁵⁷. Hg isotopic results for blood samples were validated
209 with reference values of Lake Michigan fish tissue NIST SRM 1947. Internal reference

210 samples of feathers (F-KP) and avian blood (RBC-KP) were also measured. Uncertainty
211 for delta values was calculated using 2SD typical errors for each internal reference
212 material (Table S2).

213 **Carbon and nitrogen stable isotope analyses**

214 Homogenized feather and blood subsamples (aliquots mass: ~0.3 mg) were weighed with
215 a microbalance and packed in tin containers. Carbon ($\delta^{13}\text{C}$) and nitrogen ($\delta^{15}\text{N}$) stable
216 isotope ratios were determined with a continuous flow mass spectrometer (Thermo
217 Scientific Delta V Advantage) coupled to an elemental analyser (Thermo Scientific Flash
218 EA 1112). Results are in delta notation relative to Vienna PeeDee Belemnite and
219 atmospheric N_2 for $\delta^{13}\text{C}$ and $\delta^{15}\text{N}$, respectively. Replicate measurements of internal
220 laboratory standards (acetanilide) indicated measurement errors $< 0.15\%$ for both $\delta^{13}\text{C}$
221 and $\delta^{15}\text{N}$ values. USGS-61 and USGS-62 reference materials were also analysed for
222 calibration.

223 2.3 Statistical analyses

224 Statistical analyses were performed using the software R 3.3.2 (R Core Team, 2018)⁵⁸.
225 Before statistical analyses, the data were checked for normality of distribution and
226 homogeneity of variances using Shapiro–Wilk and Breusch-Pagan tests, respectively.
227 Since data did not meet specificities of normality and homoscedasticity, non-parametrical
228 tests (Kruskal–Wallis with Conover-Iman *post-hoc* test) were performed. Statistically
229 significant results were set at $\alpha = 0.05$. Statistical significance of Hg concentration and
230 isotopic differences between head and body feathers were assessed using a randomization
231 procedure. A 99% confidence interval was calculated by means of bootstrap estimation
232 method (n=1000 iterations).

233 We examined the correlations between Hg concentrations, $\delta^{13}\text{C}$, Hg MDF ($\delta^{202}\text{Hg}$) and
234 MIF ($\Delta^{199}\text{Hg}$ and $\Delta^{200}\text{Hg}$), latitude and longitude using linear regressions and Spearman
235 correlation rank tests. The influence of the latitude and longitude of their individual
236 breeding and non-breeding distribution on feather Hg isotopic signatures were tested
237 using linear mixed models (LMMs) with colonies as random effect on the whole data set,
238 using the R package “lme4”⁵⁹. Summer latitude, summer longitude and both summer
239 latitude + longitude together were used as predictors for Hg isotopic signatures of body
240 feathers. Similarly, median winter latitude, median winter longitude and both median
241 together were used as predictors of Hg isotopic signatures in head feathers. Variance
242 inflation factors were always < 3 ⁶⁰, ensuring that there was not collinearity between
243 latitude and longitude in summer (breeding colonies) and median latitude and longitude
244 in winter (wintering areas)⁶¹. The different models were ranked based on Akaike's
245 Information Criteria adjusted for small sample sizes (AICc) and compared using ΔAICc
246 and Akaike weights (w) using the R package “wiqid”⁶². To assess the explanative power
247 of these models, marginal R^2 was obtained using the R package “r2glmm”⁶³.

248 **3 Results and discussion**

249 3.1 Seasonal and geographical variations of feather MeHg concentrations related to 250 changing foraging habits ($\delta^{15}\text{N}$)

251 We observed that the dominant fraction of Hg was in the form of MeHg both in body
252 feathers and blood ($94 \pm 2\%$, $n=20$ and $90 \pm 3\%$, $n=10$; respectively) for all the studied
253 populations of little auks (Table S3). This result is in good agreement with previous
254 studies^{55,56,64,65} and supports that both tissues of little auks principally present Hg as
255 MeHg. Body and head feathers are known to be grown at different times and therefore

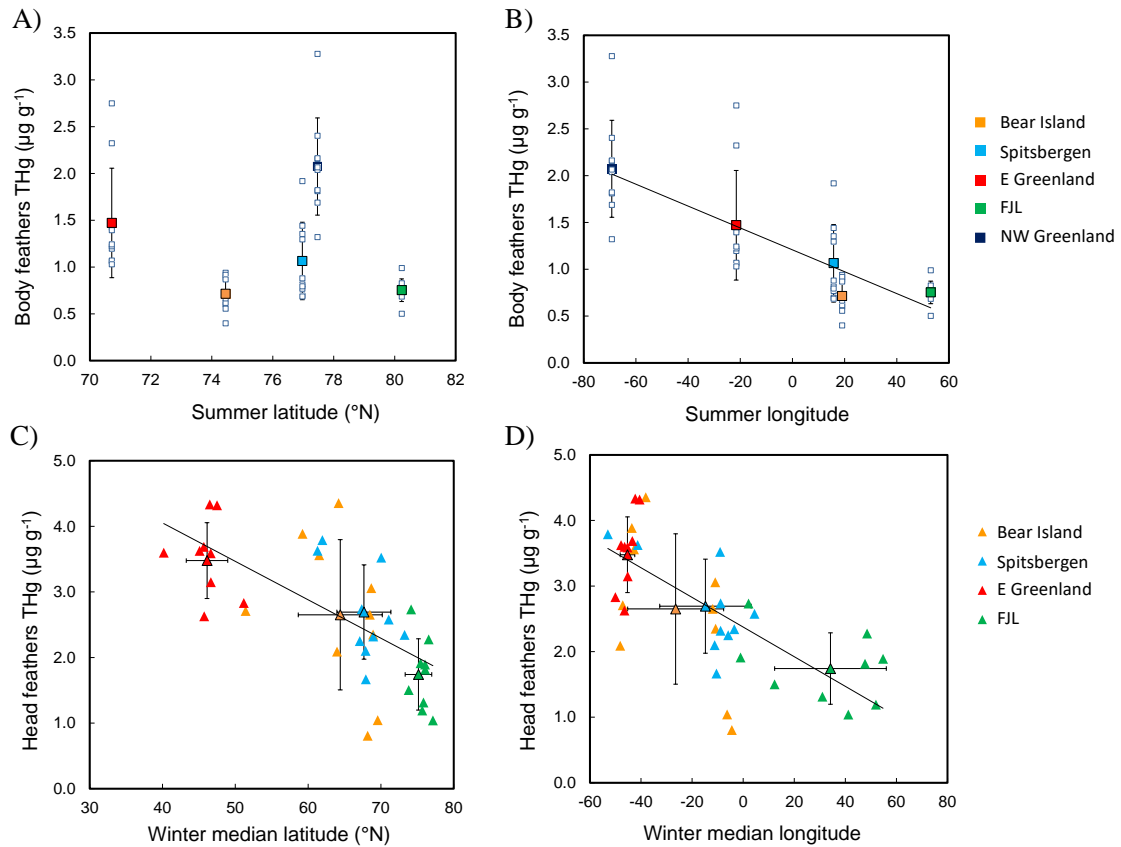
256 the Hg excreted in head and body feathers reflects respectively the exposure during their
257 wintering (October to April) and breeding (May to September) periods. Since birds are
258 known to excrete between 70 and 90% of their Hg body burden by feather moult ⁴⁸, we
259 cannot exclude that some residual Hg accumulated during the non-breeding period could
260 also be excreted during body feather moult, and vice versa, but this fraction would be
261 minor.

262 Overall, individuals presented higher Hg (MeHg) concentrations in head compared to
263 body feathers, exhibiting up to 2-fold higher concentrations in head feathers in the case
264 of East Greenland and Bear Island populations (Table S4). Higher Hg concentrations of
265 head feathers are coherent with previous observations ²² and suggest a higher exposure to
266 MeHg during the non-breeding period outside the High Arctic. For instance, little auks
267 breeding in areas of Spitsbergen and East Greenland are known to mainly forage on
268 copepods (*Calanus* spp.) during the breeding season ⁴³. However, the seasonal vertical
269 migration of their main prey *Calanus* spp. to inaccessible depths produces a seasonal shift
270 in their diet towards krill *Meganyctiphanes norvegica*, hyperiid amphipods *Themisto* spp.,
271 and fish larvae ⁶⁶. The consumption of higher trophic level prey during winter could
272 explain the higher Hg levels excreted during the spring moult (head feathers), whereas
273 they are probably less exposed to Hg in summer.

274 We also observed high variations of Hg concentrations in head feathers among
275 individuals of the same colony, especially in Bear Island (from 0.81 to 4.35 $\mu\text{g g}^{-1}$) and
276 Spitsbergen populations (from 1.67 to 3.79 $\mu\text{g g}^{-1}$) (Fig. S1). This could be due to the
277 wide-spread individual foraging specialisation during their non-breeding period and the
278 consumption of a wider range of prey ⁶⁷. Conversely, little auks occupy more restricted

279 foraging areas during the breeding season due to the need to frequently feed their chicks
280 and therefore feed on local prey captured near their respective colonies ⁶⁸, leading to less
281 intra-population variability of Hg concentrations in their body feathers.

282 We observed a consistent longitudinal trend of body feather Hg concentrations ($R^2=0.58$,
283 $p<0.0001$) with increasing Hg levels from eastern (Bear Island and FJL, 0.71 and 0.75
284 $\mu\text{g}\cdot\text{g}^{-1}$, respectively) to western colonies (NW Greenland, 2.07 $\mu\text{g}\cdot\text{g}^{-1}$) (Figure 1). When
285 applying mixed models, summer longitude was the most supported predictor of body
286 feather Hg concentrations (Table S6). Head feather Hg concentrations were positively
287 correlated both with winter latitude and longitude for the four spatially tracked
288 populations ($R^2=0.54$ and $R^2=0.60$, respectively; both $p<0.0001$) (Figure 1). Both
289 variables together were considered as predictors of Hg head feather concentrations by
290 linear mixed models (Table S7). Head feather concentrations were higher in populations
291 wintering in western zones (3.48 $\mu\text{g}\cdot\text{g}^{-1}$, East Greenland population) and decreased
292 gradually and significantly ($H=20.13$, $p=0.001$) in those wintering in northeast areas (1.74
293 $\mu\text{g}\cdot\text{g}^{-1}$, FJL population). The consistent longitudinal patterns both in summer and winter
294 reflect a higher accumulation of MeHg in little auks from western regions, whereas
295 colonies breeding in Arctic northern regions seem to be exposed to lower concentrations.



296

297 **Figure 1. Hg concentration ($\mu\text{g}\cdot\text{g}^{-1}$) of little auk body feathers (summer) as a function of**
 298 **latitude (A) and longitude of their breeding sites (B) and head feathers (winter) as a function**
 299 **of the median latitude (C) and longitude (D) of their winter grounds. Regression lines are**
 300 **A) Slope: 0.052 ± 0.013 , intercept: -3.420 ± 0.997 , $R^2=0.26$, $p=0.005$; B) Slope: -0.012 ± 0.001 ,**
 301 **intercept: 1.209 ± 0.059 , $R^2=0.58$, $p<0.0001$; C) Slope: -0.059 ± 0.011 , intercept: 6.399 ± 0.669 ,**
 302 **$R^2=0.54$, $p<0.0001$; D) Slope: -0.022 ± 0.003 , intercept: 2.375 ± 0.120 , $R^2=0.60$, $p<0.0001$.**
 303 **Regression lines presented only for significant relationship between the two variables.**

304

305 Seabird blood $\delta^{15}\text{N}$ values provide short- to medium-term information (about 1–5 weeks)
 306 while feathers $\delta^{15}\text{N}$ values reflect the diet at the time they were grown^{50,69}. The
 307 distribution of little auk populations in winter was limited to the North Atlantic and the
 308 Arctic areas, where large-scale $\delta^{15}\text{N}$ values are known to be relatively homogeneous at
 309 the base of the food web^{70,71}, then allowing the inter-population comparison. The lower

310 body feather Hg concentrations and blood $\delta^{15}\text{N}$ values observed in little auks (Table S5)
311 suggest that all birds from the different populations mostly feed at low trophic levels and
312 on *Calanus* copepods in summer. Contrarily, the interpopulation differences of $\delta^{15}\text{N}$
313 values in winter (head feathers) were much more pronounced (Table S4). For instance,
314 little auk populations breeding in FJL and Bear Island exhibited a ~ 3 ‰ higher $\delta^{15}\text{N}$
315 values in head feathers than in blood. This difference highlights the spatial variability of
316 $\delta^{15}\text{N}$ values in relation to the different winter distribution of little auks in winter. Previous
317 studies have reported significant seasonal variations in copepod $\delta^{15}\text{N}$ values (up to 6‰)
318 between late winter and spring (highly productive periods) relative to the summer and
319 autumn periods^{71,72}. The seasonal variability of zooplankton $\delta^{15}\text{N}$ values is common on
320 the eastern and western parts of the North Atlantic Ocean and needs to be considered here
321 due to the wide spatial distribution of little auks in winter. Therefore, the higher feather
322 Hg concentrations little auk colonies from western parts of the Arctic Ocean could be
323 influenced by their seasonal dietary shifts and different spatial distribution but also by the
324 complex Hg oceanic dynamics or distinct environmental sources that control the level of
325 exposure to MeHg at the different regions.

326 3.2 Spatio-temporal trends of Hg MDF ($\delta^{202}\text{Hg}$) in feathers related to ecological aspects

327 Specific Hg integration times of seabird tissues may influence the seasonal incorporation
328 of MeHg from different spatial origin⁷³. However, the geographical variations in $\delta^{202}\text{Hg}$
329 values are generally difficult to distinguish since metabolic processes also induce Hg
330 MDF. Head and body feathers showed large ranges of $\delta^{202}\text{Hg}$ values, varying from -0.24
331 to 1.43 ‰ and from -0.11 to 1.28 ‰, respectively. Although we focused on the study of
332 multiple colonies of the same seabird species to minimize the metabolic or trophic-related
333 effects, we cannot exclude that the variability of $\delta^{202}\text{Hg}$ signatures among colonies is led

334 only by the specific isotopic baseline of their respective foraging habitats. For instance,
335 FJL population exhibited significantly heavier $\delta^{202}\text{Hg}$ values relative to the other four
336 populations, both in head ($H=29.42$, $p<0.0001$) and body feathers ($H=27.69$, $p<0.0001$)
337 (Table S4). It is known that little auks from FJL are morphologically bigger than those of
338 the populations from Svalbard due to more severe climate conditions in this area ⁷⁴. Thus,
339 potentially different morphological characteristics associated to their bigger size could
340 contribute to higher feather $\delta^{202}\text{Hg}$ values in this colony. Hg concentrations and $\delta^{202}\text{Hg}$
341 values of head feathers were highly correlated for the overall populations ($R^2=0.52$,
342 $p<0.0001$), while $\Delta^{199}\text{Hg}$ signatures were not related to Hg concentration in any type of
343 feather (Figure S2). This observation shows the completely decoupled behavior between
344 $\delta^{202}\text{Hg}$ and $\Delta^{199}\text{Hg}$ signatures. The influence of biological and ecological factors on
345 $\delta^{202}\text{Hg}$ values shows the limitation of this type of signature to discern spatial MeHg
346 sources related to different migratory routes of seabird populations. The utilisation of
347 feather $\delta^{202}\text{Hg}$ values as a proxy of geographical patterns or to changing environmental
348 conditions requires a complete knowledge of all the processes and factors driving Hg
349 MDF (i.e., trophic ecology and intrinsic metabolic/physiological processes).

350 3.3 Hg odd-MIF ($\Delta^{199}\text{Hg}$): seasonal and spatial differences of Hg marine 351 photochemistry

352 Head and body feather odd-MIF values ($\Delta^{199}\text{Hg}$) ranged from 0.72 to 1.26 ‰ and 0.90 to
353 1.91 ‰, respectively. Significantly higher $\Delta^{199}\text{Hg}$ values in body compared to head
354 feathers (Table S8) suggest a seasonal variability in odd-MIF values. This could be
355 primarily associated to the vertical migration of little auk main prey (copepods) and the
356 consequent seasonal shift on their diet to krill/amphipods during the winter season. Their
357 seasonal diet shift could enhance the accumulation of pelagic MeHg that is less connected

358 to the photic zone during winter, then leading to lower $\Delta^{199}\text{Hg}$ values of the MeHg
359 excreted into head feathers. A previous study on subantarctic penguins documented
360 significant differences of $\Delta^{199}\text{Hg}$ values as a function of their specific foraging depths ²⁴,
361 increasing around 0.4 ‰ from benthic to epipelagic populations. Although the little auk
362 populations studied here are known to mainly feed on the same prey items and forage at
363 similar depths, we should consider that changes on the availability of their prey among
364 sites could also contribute to different feather $\Delta^{199}\text{Hg}$ values among populations. Further,
365 due to the diurnal migration of zooplankton from deep water to the surface, the mixed
366 pool of Hg accumulated in these organisms originate from different depths of the water
367 column and therefore, their $\Delta^{199}\text{Hg}$ values represent a mixture from deep (low
368 photodemethylated) Hg and surface Hg uptake ⁷⁵. Together with the trophic and
369 ecological factors, we could expect that the seasonal variability of feather $\Delta^{199}\text{Hg}$ values
370 (body vs head feathers) of little auks could be also influenced by a higher extent of Hg
371 marine photochemistry occurring during summer. In summertime/ spring, little auks are
372 known to return to their breeding sites, located at northern latitudes, where they are
373 exposed to longer daily photoperiod at this moment of the year (polar day). Nevertheless,
374 the weak differences of $\Delta^{199}\text{Hg}$ values between body and head feathers of a same
375 population (from 0.26 to 0.50 ‰, [Table S8](#)) seem to indicate low variations of MeHg
376 photodemethylation extents between their summer and winter sites. Therefore, the
377 differences on daily photoperiod and/or light penetration between their summer and
378 wintering foraging grounds would have a minor role on Hg isotopic variations.

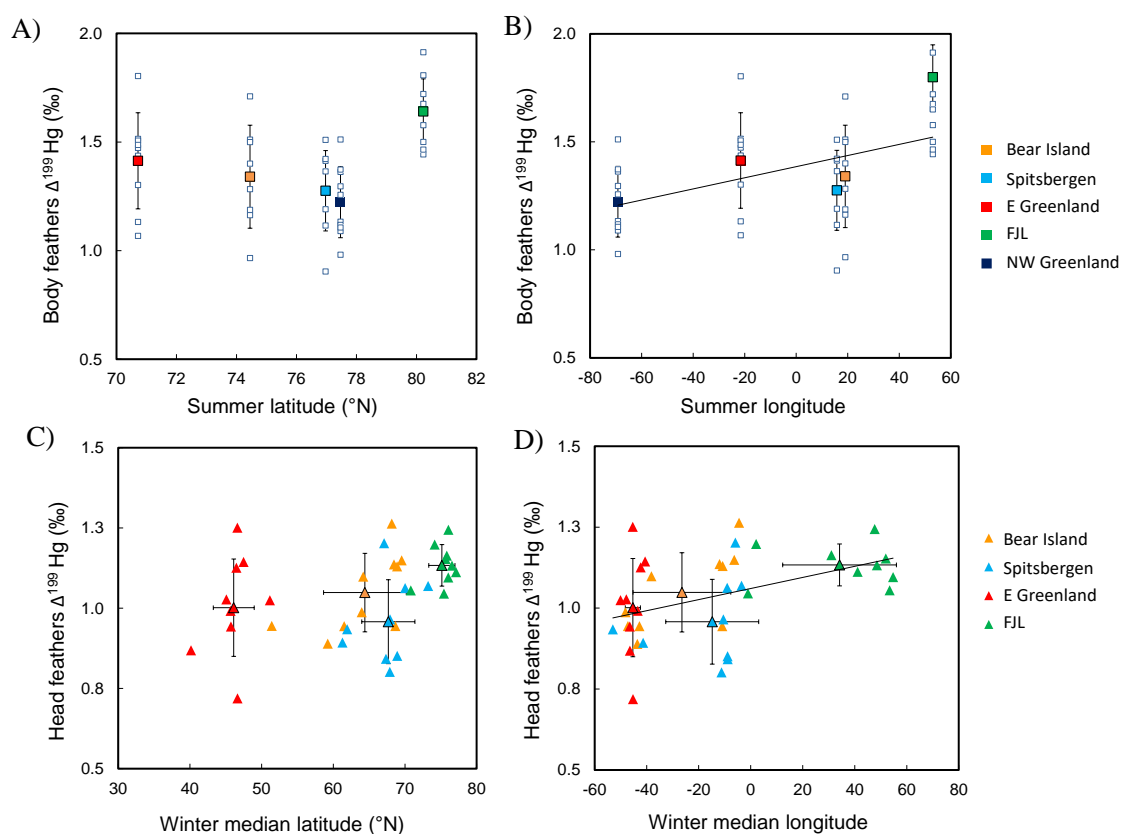
379 Concerning the spatial variability of $\Delta^{199}\text{Hg}$ values among colonies, we observed positive
380 linear relationships between body feather $\Delta^{199}\text{Hg}$ values and summer longitude ($R^2=0.20$,
381 $p<0.0001$) and between head feather $\Delta^{199}\text{Hg}$ values and winter longitude ($R^2=0.22$,

382 $p < 0.0001$) (Figure 2). Summer and winter longitudes were respectively the most
383 supported explanatory factors of body and head feather $\Delta^{199}\text{Hg}$ values (Tables S6 and
384 S7). No significant relationships were observed with latitude in summer ($R^2=0.01$,
385 $p=0.20$) nor winter ($R^2=0.07$, $p=0.06$) (Figure 2). FJL population, the northern colony of
386 this study, showed slightly higher body feather $\Delta^{199}\text{Hg}$ values ($1.64 \pm 0.15 \text{ ‰}$, $n=10$,
387 80°N) comparing to other studied colonies ($1.31 \pm 0.20 \text{ ‰}$, $n=37$ $70\text{-}77^\circ\text{N}$) ($H=11.96$,
388 $p=0.018$). FJL individuals also presented higher $\Delta^{199}\text{Hg}$ values of their head feathers (1.13
389 $\pm 0.06 \text{ ‰}$) compared to the other colonies ($1.00 \pm 0.12 \text{ ‰}$) ($H=18.55$, $p=0.001$). Previous
390 studies on Alaskan seabirds reported around 2-fold higher mean $\Delta^{199}\text{Hg}$ signatures in low-
391 ice-covered oceanic areas ($1.13 \pm 0.16 \text{ ‰}$; $56\text{-}58^\circ\text{N}$) than highly ice-covered regions (0.53
392 $\pm 0.15 \text{ ‰}$; 68°N) and revealed that the presence of sea ice inhibits light penetration and
393 therefore, Hg marine photochemistry²⁵. Compared to the latitudinal trend observed in
394 Alaska, the spatial variations of $\Delta^{199}\text{Hg}$ values between northern and southern populations
395 of little auks are relatively weak and, interestingly, presented an inversed tendency
396 between highly ice-covered (FJL) and non-ice-covered areas (North Atlantic regions).
397 Therefore, we cannot presume that the presence of sea ice is a driving factor controlling
398 MeHg photochemistry and the related odd-MIF signatures registered in feathers of little
399 auks. The existence of an opposed north-to-south trend of $\Delta^{199}\text{Hg}$ values between the
400 Eastern and Western Arctic Ocean regions reveals different Hg dynamic systems,
401 especially for Hg accumulation pathways in food webs.

402 According to previous findings, the largest MeHg production in the Arctic water column
403 seems to occur in oxic surface waters just below the productive surface layer^{6,13}. In the
404 Arctic, additional sources of Hg and carbon are provided by sea ice algae during spring
405 blooms⁷⁶. The presence of terrestrial organic matter and sea ice layers that concentrates

406 phytoplankton near the MeHg production zone may favour the Hg microbial methylation
407 at shallow depths of the Arctic water column ^{12,77}. Shallower methylation occurring in
408 Arctic waters may result in higher photochemical impact on MeHg before its assimilation
409 in Arctic biota compared to North Atlantic marine food webs. This phenomenon could
410 contribute to the higher feather $\Delta^{199}\text{Hg}$ values of FJL little auks compared to populations
411 breeding at lower latitudes. The slight differences of $\Delta^{199}\text{Hg}$ values between northern and
412 southern colonies of little auks are similar to the ranges recently observed in seabirds
413 covering a wider latitudinal gradient (37 to 66°S) in the Southern Ocean, for which $\Delta^{199}\text{Hg}$
414 values increased from Antarctic (1.31 to 1.73 ‰) to subtropical (1.69 to 2.04 ‰)
415 populations ⁷⁸. The slight variations of $\Delta^{199}\text{Hg}$ values also found between these distant
416 sites of the Southern Ocean were translated into low differences of MeHg photochemical
417 demethylation extents among sites and a dominance of MeHg with a mesopelagic origin
418 in these remote environments. As previously discussed, the vertical daily migration of
419 copepods from deep water to the surface leads to the integration of Hg from relatively
420 deep zones of the water column therefore, contributing to the incorporation of low
421 photochemically impacted Hg in consumers ⁷⁵. Therefore, although the planktivorous
422 little auk feed at surface waters on the photic zone, their relatively low feather $\Delta^{199}\text{Hg}$
423 values suggest that the Hg accumulated in their main prey could originate from Hg pools
424 from deeper zones of the water column.

425



426

427 **Figure 2. Hg odd-MIF ($\Delta^{199}\text{Hg}$) of little auk body feathers (summer) as a function of latitude (A) and**
 428 **longitude of their breeding sites (B) and head feathers (winter) as a function of the median latitude**
 429 **(C) and longitude (D) of their wintering grounds. Regression lines are A) Slope: 0.014 ± 0.011 ,**
 430 **intercept: 0.319 ± 0.822 ; $R^2=0.01$, $p=0.20$; B) Slope: 0.002 ± 0.001 , intercept: 1.384 ± 0.031 , $R^2=0.20$,**
 431 **$p<0.0001$; C) Slope: 0.004 ± 0.002 , intercept: 0.784 ± 0.123 , $R^2=0.07$, $p=0.06$; D) Slope: 0.001 ± 0.001 ,**
 432 **intercept: 1.069 ± 0.022 , $R^2=0.22$, $p=0.002$. Regression lines presented only for significant relationship**
 433 **between the two variables.**

434

435 3.4 Spatial correlation of Hg MIF signatures and carbon stable isotopes ($\delta^{13}\text{C}$)

436 The deposition of atmospheric Hg from mid-latitude anthropogenic emissions into the
 437 Arctic Ocean could contribute to the accumulation of MeHg from distinct origin in Arctic-
 438 North Atlantic food webs⁷. Although body feathers of little auk presented a relative high
 439 range of $\Delta^{200}\text{Hg}$ signatures (from -0.23 to 0.17 ‰), the inter-population differences were
 440 not significant ($H=3.685$, $p=0.45$) (Figure S5). No substantial interpopulation variations

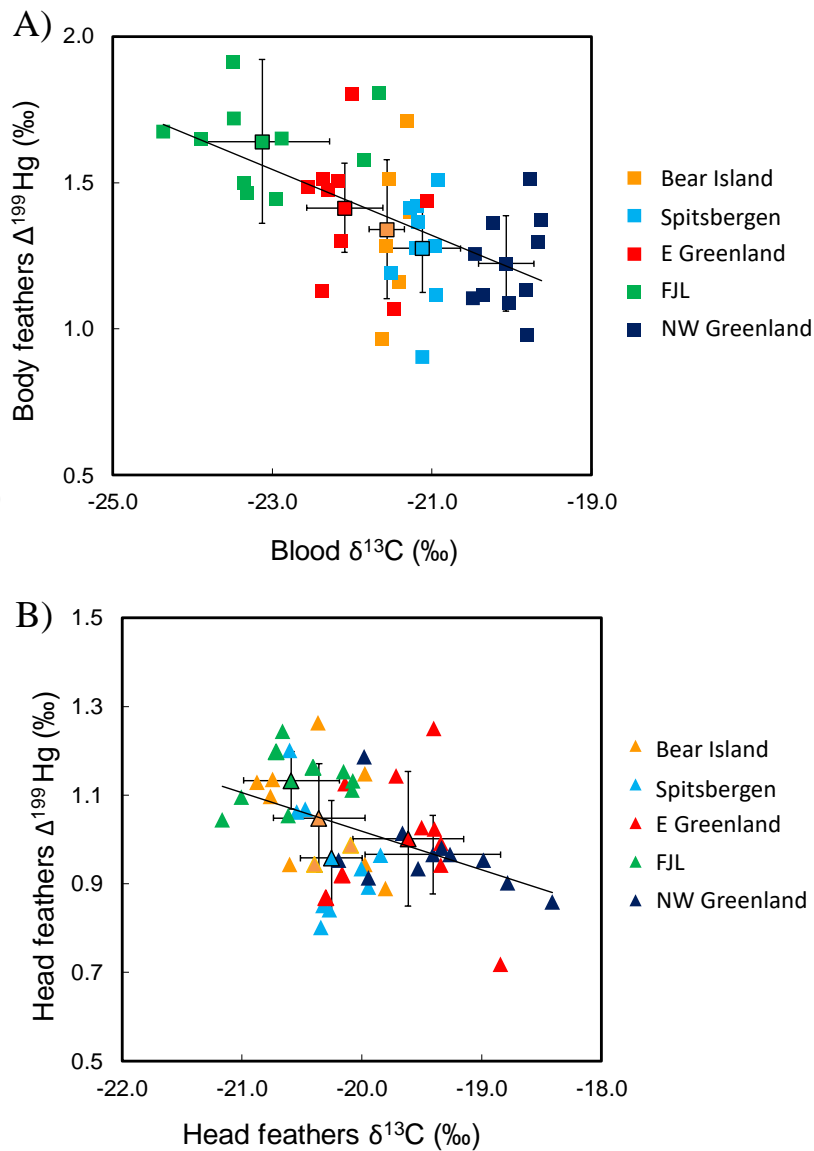
441 of $\Delta^{200}\text{Hg}$ values were neither observed for head feathers of little auks (-0.14 to 0.12 ‰),
442 therefore we cannot discriminate Hg sources from distinct atmospheric origin among
443 seabird wintering grounds. Nevertheless, the spatial trends of $\Delta^{200}\text{Hg}$ values observed in
444 little auks are more variable than those previously reported on Arctic marine mammals
445 and seabirds of Alaska (from -0.01 to 0.10 ‰; 71 to 54 °N⁷⁹) and on Antarctic and
446 subtropical seabirds (from -0.02 to 0.04 ‰, 66 to 37 °S⁷⁸).

447 Large-scale ocean circulation and vertical transport processes throughout the water
448 column could influence the distribution of distinct MeHg sources between the widely
449 distributed compartments used by little auks. The exploration of carbon stable isotopes
450 ($\delta^{13}\text{C}$) of little auks could help discriminating the potential contributions of distinct MeHg
451 sources linked to the widely specific foraging habitats of little auks. Contrary to Hg
452 isotopes, body feather $\delta^{13}\text{C}$ values do not reflect the period of summer but the moult
453 period in late summer/early autumn (September) when they are grown⁴⁵. To ensure only
454 the integration of the summer, breeding period, we compared body feather Hg isotopes
455 with blood $\delta^{13}\text{C}$ values. Little auks from FJL exhibited the lowest blood $\delta^{13}\text{C}$ values (-
456 23.13 ± 0.84 ‰) and NW Greenland individuals the highest (-20.07 ± 0.35 ‰) relative to
457 the rest of the colonies ($H=40.74$, $p<0.0001$) (Table S5). Head feather $\delta^{13}\text{C}$ values
458 separated little auk populations in those overwintering in western areas of the North
459 Atlantic Ocean and those wintering in north-eastern areas ($H=26.28$, $p<0.0001$). The
460 gradient of $\delta^{13}\text{C}$ values of head feathers increased from populations of FJL (-20.59 ± 0.40
461 ‰) and Bear Island (-20.35 ± 0.38 ‰), to Northwest (-19.41 ± 0.57 ‰) and East
462 Greenland (-19.61 ± 0.46 ‰) populations. Latitudinal gradients of $\delta^{13}\text{C}$ values of the
463 dissolved inorganic carbon are commonly observed in surface waters as an influence of
464 the physical and biological processes⁷¹. For instance, it is known that CO_2 solubility is

465 favoured in cold oceanic waters and consequently, surface waters at high latitudes have
466 relatively low $\delta^{13}\text{C}$ values due to the introduction of isotopically light atmospheric CO_2 .
467 By contrast, surface waters of outgassing upwelling equatorial areas become enriched on
468 $\delta^{13}\text{C}$ values^{80,81}. Parallely, the $\delta^{13}\text{C}$ values of primary producers are strongly influenced
469 by the $\delta^{13}\text{C}$ values of dissolved inorganic carbon and therefore, by the temperature
470 gradients and CO_2 solubility⁷¹. Spatial gradients of sea surface temperature and CO_2
471 concentrations could thus explain the more depleted $\delta^{13}\text{C}$ baseline in cold high Arctic
472 marine food webs and the enrichment in $\delta^{13}\text{C}$ values when going southward to North
473 Atlantic oceanic areas. Furthermore, the dominance of distinct marine currents between
474 the different wintering seabird sites could strongly determine the $\delta^{13}\text{C}$ at the base of the
475 food webs. The FJL archipelago and surrounding high Arctic areas are strongly impacted
476 by the Makarov and Arctic cold currents flowing southward from the north, and
477 potentially contributing to transport isotopically depleted carbon from high latitude areas.
478 In contrast, little auk wintering regions near the Newfoundland Island (East and West
479 Greenland populations) are affected by the Gulf Stream and North Atlantic Current⁴⁵
480 which could supply carbon organic matter from warmer water masses⁸².

481 Significant negative linear relationships were obtained between $\Delta^{199}\text{Hg}$ and $\delta^{13}\text{C}$ values
482 both in summer ($R^2=0.17$, $p=0.003$) and winter ($R^2=0.31$, $p<0.0001$) (Figure 3).
483 Interestingly, the negative relationship between $\Delta^{199}\text{Hg}$ and $\delta^{13}\text{C}$ values of little auks
484 contrasts with those previously reported on eggs from guillemot species (or murre, *Uria*
485 *aalge* and *U. lomvia*) breeding in the Alaskan Arctic²⁶. These authors reported a co-
486 enrichment of egg $\delta^{13}\text{C}$ and $\Delta^{199}\text{Hg}$ values linked to the transition from terrestrial to
487 marine Hg sources and the subsequent reduction of Hg photochemistry in coastal
488 reservoirs due to higher turbidity²⁶. However, the wintering areas of little auks mainly

489 correspond to more opened oceanic areas as the study in the Bering Sea and probably do
490 not present such a remarkable coastal-oceanic gradient. The significant correlation
491 obtained here between $\Delta^{199}\text{Hg}$ and $\delta^{13}\text{C}$ signatures both in body and head feathers of little
492 auks reflect common spatial trends summer and winter foraging grounds. This interesting
493 relationship seems be associated to both the spatial gradient of physical parameters
494 controlling C isotopic baselines (temperature and CO_2 exchange in surface waters) and to
495 the extent of Hg photochemical processes. Probably, a higher stratification and impact of
496 sea ice cover in high Arctic oceanic zones favours the methylation of Hg in surface waters
497 ¹³, and the extent of photochemical reactions leading to slightly positive $\Delta^{199}\text{Hg}$ values
498 and more negative $\delta^{13}\text{C}$ values of biota. The dominance of northern marine currents in
499 this area would also contribute to depleted $\delta^{13}\text{C}$ values. Although we could consider the
500 existence of distinct carbon inputs transported by the marine currents on these ecosystems
501 (i.e. external carbon supply, planktonic production), the complex interaction of
502 oceanographic and physical parameters governing these areas does not allow to provide
503 conclusive evidence from our data.



504

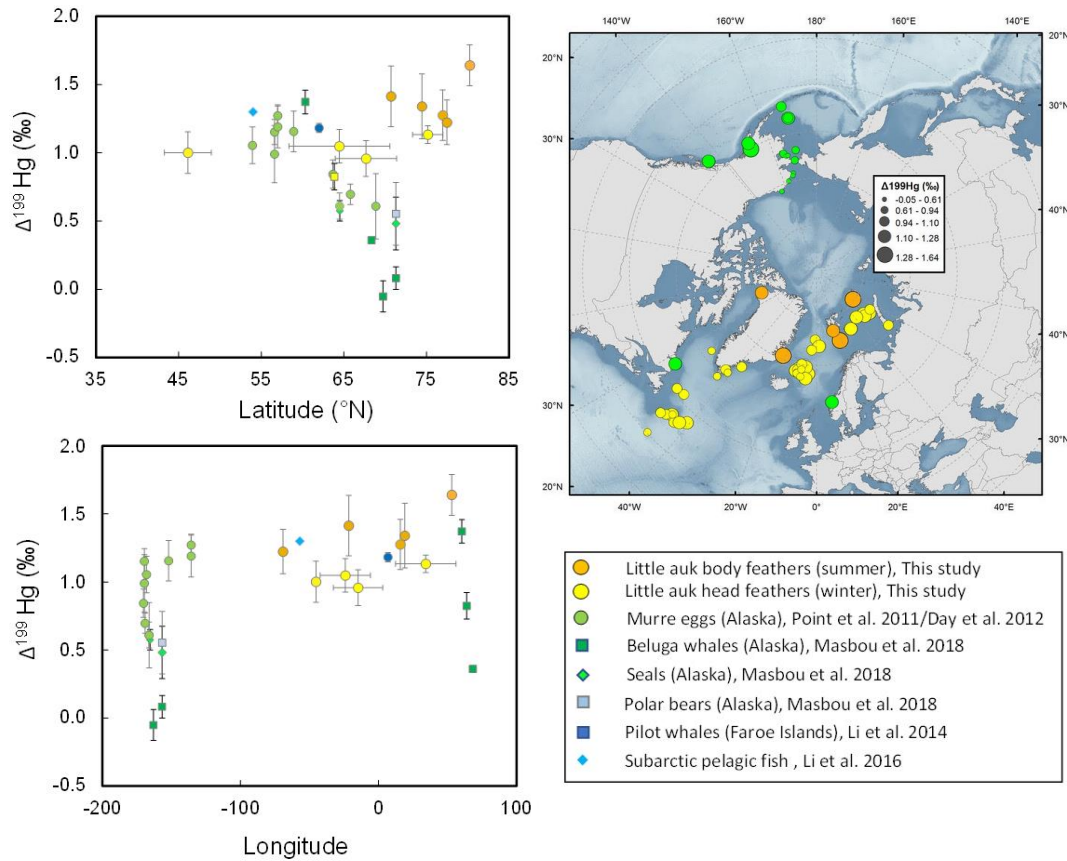
505 **Figure 3. Carbon ($\delta^{13}\text{C}$) vs MIF Hg signatures for A) summer (body feathers) and B) winter (head**
 506 **feathers) periods. Regression lines are A) Slope: -0.122 ± 0.026 , intercept: -1.045 ± 0.558 , $R^2=0.31$,**
 507 **$p < 0.0001$; B) Slope: -0.088 ± 0.028 , intercept: -0.746 ± 0.566 , $R^2=0.17$, $p=0.003$.**

508 3.5 Geographically distinct Hg source mixing across the Arctic and North Atlantic
 509 Oceans

510 Our results suggest that the variations in relation to longitude of the Hg concentrations,
 511 $\Delta^{199}\text{Hg}$, and $\delta^{13}\text{C}$ values of little auks is linked to the assimilation of isotopically distinct
 512 MeHg depending on their wintering grounds. Figure 4 shows a compilation of Hg odd-

513 MIF values observed in little auks compared to previous studies in Arctic biota over a
514 wide spatial scale. The observed isotopic spatial variability across the different regions of
515 the Arctic Ocean suggests the existence of two different Hg systems between East
516 (Atlantic) and West (Pacific) Arctic Ocean regions. Our opposed trend of $\Delta^{199}\text{Hg}$ from
517 north to south populations values relative to Western Arctic compartments ^{25,35} indicates
518 that the presence of sea ice cover is not the only driving factor controlling Hg
519 photochemistry in the Eastern Arctic Ocean. Possibly, an additional supply of Hg and
520 carbon sources by sea-ice algae may enhance the microbial/photochemical methylation
521 and demethylation processes at shallower depths ^{6,13} in East Arctic regions, therefore
522 contributing to the higher odd-MIF values of Hg accumulated in biota. The inversed
523 relationship of $\Delta^{199}\text{Hg}$ and $\Delta^{200}\text{Hg}$ values of little auks with latitude is opposed to the
524 latitudinal covariation of $\Delta^{199}\text{Hg}$ and $\Delta^{200}\text{Hg}$ in biota from Western Arctic regions ⁷⁹ and
525 from Antarctic regions ⁷⁸ and evidences a completely different functioning of Hg cycling
526 compared to other polar marine environments. Complex Hg dynamics and ocean control
527 factors seem to drive the increasing pattern of Hg isotopes from west to east regions of
528 the Arctic Ocean. Future research assessing large scale and long-term Hg contamination
529 are necessary to have a complete understanding of the Hg exposure pathways and of the
530 associated risks for the whole marine Arctic environments.

531



532

533 **Figure 4. Compilation of Hg odd-MIF values ($\Delta^{199}\text{Hg}$) of marine biota from spatially distant Arctic**
 534 **Regions. The map comprises both little auk breeding sites (orange), individual little auk median**
 535 **winter positions (yellow) and previous published data (green) including seabirds ^{25,26}, beluga whale,**
 536 **seals and polar bears ⁷⁹ from Alaskan Regions; pilot whales from Faroe Islands ²⁸, and fish from the**
 537 **Labrador Sea ⁸³.**

538

539 Acknowledgements

540 The authors wish to thank the fieldworkers who collected the samples. Field procedures
 541 were authorized by the Ethics Committee of Institut Polaire Français Paul Emile Victor
 542 (IPEV) and by the Comité de l'Environnement Polaire. This study received financial and
 543 logistical support from the French Agency for National Research (ANR MAMBA project
 544 ANR-16-TERC-0004, ILETOP project ANR-16-CE34-0005), the French Arctic

545 Initiative - CNRS (PARCS project), the Mission pour l'Interdisciplinarité - CNRS
546 (Changements en Sibérie project) and the French Polar Institute (IPEV - Pgr 388
547 ADACLIM). The IUF (Institut Universitaire de France) is also acknowledged for its
548 support to PB as a senior member.

549

550 **References**

- 551 (1) Tan, S. W.; Meiller, J. C.; Mahaffey, K. R. The Endocrine Effects of Mercury in Humans
552 and Wildlife. *Crit. Rev. Toxicol.* **2009**, *39* (3), 228–269.
553 <https://doi.org/10.1080/10408440802233259>.
- 554 (2) Lehnher, I.; St. Louis, V. L.; Hintelmann, H.; Kirk, J. L. Methylation of Inorganic
555 Mercury in Polar Marine Waters. *Nat. Geosci.* **2011**, *4* (April), 298–302.
556 <https://doi.org/10.1038/ngeo1134>.
- 557 (3) Blum, J. D.; Popp, B. N.; Drazen, J. C.; Anela Choy, C.; Johnson, M. W. Methylmercury
558 Production below the Mixed Layer in the North Pacific Ocean. *Nat. Geosci.* **2013**, *6* (10),
559 879–884. <https://doi.org/10.1038/ngeo1918>.
- 560 (4) Mason, R. P.; Choi, A. L.; Fitzgerald, W. F.; Hammerschmidt, C. R.; Lamborg, C. H.;
561 Soerensen, A. L.; Sunderland, E. M. Mercury Biogeochemical Cycling in the Ocean and
562 Policy Implications. *Environ. Res.* **2012**, *119*, 101–117.
563 <https://doi.org/10.1016/j.envres.2012.03.013>.
- 564 (5) Bowman, K. L.; Lamborg, C. H.; Agather, A. M. A Global Perspective on Mercury
565 Cycling in the Ocean. *Sci. Total Environ.* **2020**, *710*, 136166.
566 <https://doi.org/10.1016/j.scitotenv.2019.136166>.
- 567 (6) Soerensen, A. L.; Jacob, D. J.; Schartup, A. T.; Fisher, J. A.; Lehnher, I.; Louis, V. L. S.;

- 568 Heimbürger, L.; Sonke, J. E.; Krabbenhoft, D. P.; Sunderland, E. M. A Mass Budget for
569 Mercury and Methylmercury in the Arctic Ocean. *Global Biogeochem. Cycles* **2016**, *30*
570 (4), 560–575. <https://doi.org/10.1002/2015GB005280>.
- 571 (7) Larose, C.; Dommergue, A.; Maruszczak, N.; Coves, J.; Ferrari, C. P.; Schneider, D.
572 Bioavailable Mercury Cycling in Polar Snowpacks. *Environ. Sci. Technol.* **2011**, *45*,
573 2150–2156. <https://doi.org/10.1021/es103016x>.
- 574 (8) Beattie, S. A.; Armstrong, D.; Chaulk, A.; Comte, J.; Gosselin, M.; Wang, F. Total and
575 Methylated Mercury in Arctic Multiyear Sea Ice. *Environ. Sci. Technol.* **2014**, *48* (10),
576 5575–5582. <https://doi.org/10.1021/es5008033>.
- 577 (9) Sonke, J. E.; Teisserenc, R.; Heimbürger-Boavida, L.-E.; Petrova, M. V.; Maruszczak, N.;
578 Le Dantec, T.; Chupakov, A. V.; Li, C.; Thackray, C. P.; Sunderland, E. M.; Tananaev,
579 N.; Pokrovsky, O. S. Eurasian River Spring Flood Observations Support Net Arctic Ocean
580 Mercury Export to the Atmosphere and Atlantic Ocean. *Proc. Natl. Acad. Sci.* **2018**,
581 201811957. <https://doi.org/10.1073/pnas.1811957115>.
- 582 (10) Obrist, D.; Agnan, Y.; Jiskra, M.; Olson, C. L.; Dominique, P.; Hueber, J.; Moore, C. W.;
583 Sonke, J.; Helmig, D. Tundra Uptake of Atmospheric Elemental Mercury Drives Arctic
584 Mercury Pollution. *Nat. Publ. Gr.* **2017**, *547* (7662), 201–204.
585 <https://doi.org/10.1038/nature22997>.
- 586 (11) Kirk, J.; St. Louis, V. L.; Hintelmann, H.; Lehnher, I.; Else, B.; Poissant, L. Methylated
587 Mercury Species in Marine Waters of the Canadian High and Sub Arctic. *Env. Sci Technol*
588 **2008**, *42* (22), 8367–8373. <https://doi.org/https://doi.org/10.1021/es801635m>.
- 589 (12) Gionfriddo, C. M.; Tate, M. T.; Wick, R. R.; Schultz, M. B.; Zemla, A.; Thelen, M. P.;
590 Schofield, R.; Krabbenhoft, D. P.; Holt, K. E.; Moreau, J. W. Microbial Mercury
591 Methylation in Antarctic Sea Ice. *Nat. Microbiol.* **2016**, *1* (10), 16127.

- 592 <https://doi.org/10.1038/nmicrobiol.2016.127>.
- 593 (13) Heimbürger, L. E.; Sonke, J. E.; Cossa, D.; Point, D.; Lagane, C.; Laffont, L.; Galfond, B.
594 T.; Nicolaus, M.; Rabe, B.; van der Loeff, M. R. Shallow Methylmercury Production in
595 the Marginal Sea Ice Zone of the Central Arctic Ocean. *Sci. Rep.* **2015**, *5*, 10318.
596 <https://doi.org/10.1038/srep10318>.
- 597 (14) Villar, E.; Cabrol, L.; Heimbürger-Boavida, L. E. Widespread Microbial Mercury
598 Methylation Genes in the Global Ocean. *Environ. Microbiol. Rep.* **2020**, *12* (3).
599 <https://doi.org/10.1111/1758-2229.12829>.
- 600 (15) AMAP. *Arctic Monitoring and Assessment Program 2011: Mercury in the Arctic*; 2011.
- 601 (16) AMAP. *AMAP Assessment 2018: Biological Effects of Contaminants on Arctic Wildlife*
602 *and Fish*; 2018.
- 603 (17) Thompson, D. R.; Furness, R. W.; Walsh, P. M. Historical Changes in Mercury
604 Concentrations in the Marine Ecosystem of the North and North-East Atlantic Ocean as
605 Indicated by Seabird Feathers. *J. Appl. Ecol.* **1992**, *29* (1), 79–84.
606 <https://doi.org/10.2307/2404350>.
- 607 (18) Carravieri, A.; Cherel, Y.; Jaeger, A.; Churlaud, C.; Bustamante, P. Penguins as
608 Bioindicators of Mercury Contamination in the Southern Indian Ocean: Geographical and
609 Temporal Trends. *Environ. Pollut.* **2016**, *213*, 195–205.
610 <https://doi.org/10.1016/j.envpol.2016.02.010>.
- 611 (19) Rigét, F.; Braune, B.; Bignert, A.; Wilson, S.; Aars, J.; Born, E.; Dam, M.; Dietz, R.;
612 Evans, M.; Evans, T.; Gamberg, M.; Gantner, N.; Green, N.; Gunnlaugsdóttir, H.; Kannan,
613 K.; Letcher, R.; Muir, D.; Roach, P.; Sonne, C.; Stern, G.; Wiig, O. Temporal Trends of
614 Hg in Arctic Biota, an Update. *Sci. Total Environ.* **2011**, *409* (18), 3520–3526.
615 <https://doi.org/10.1016/j.scitotenv.2011.05.002>.

- 616 (20) Dietz, R.; Sonne, C.; Basu, N.; Braune, B.; O'Hara, T.; Letcher, R. J.; Scheuhammer, T.;
617 Andersen, M.; Andreassen, C.; Andriashek, D.; Asmund, G.; Aubail, A.; Baagøe, H.; Born,
618 E. W.; Chan, H. M.; Derocher, A. E.; Grandjean, P.; Knott, K.; Kirkegaard, M.; Krey, A.;
619 Lunn, N.; Messier, F.; Obbard, M.; Olsen, M. T.; Ostertag, S.; Peacock, E.; Renzoni, A.;
620 Rigét, F. F.; Skaare, J. U.; Stern, G.; Stirling, I.; Taylor, M.; Wiig, Ø.; Wilson, S.; Aars, J.
621 What Are the Toxicological Effects of Mercury in Arctic Biota? *Sci. Total Environ.* **2013**,
622 *443*, 775–790. <https://doi.org/10.1016/j.scitotenv.2012.11.046>.
- 623 (21) Albert, C.; Renedo, M.; Bustamante, P.; Fort, J. Using Blood and Feathers to Investigate
624 Large-Scale Hg Contamination in Arctic Seabirds: A Review. *Environ. Res.* **2019**, *177*
625 (July), 108588. <https://doi.org/10.1016/j.envres.2019.108588>.
- 626 (22) Fort, J.; Robertson, G. J.; Grémillet, D.; Traisnel, G.; Bustamante, P. Spatial
627 Ecotoxicology: Migratory Arctic Seabirds Are Exposed to Mercury Contamination While
628 Overwintering in the Northwest Atlantic. *Environ. Sci. Technol.* **2014**, *48* (11560–11567).
629 <https://doi.org/10.1021/es504045g>.
- 630 (23) Fleishman, A. B.; Orben, R. A.; Kokubun, N.; Will, A.; Paredes, R.; Ackerman, J. T.;
631 Takahashi, A.; Kitaysky, A. S.; Shaffer, S. A. Wintering in the Western Subarctic Pacific
632 Increases Mercury Contamination of Red-Legged Kittiwakes. *Environ. Sci. Technol.*
633 **2019**, *53* (22), 13398–13407. <https://doi.org/10.1021/acs.est.9b03421>.
- 634 (24) Renedo, M.; Amouroux, D.; Pedrero, Z.; Bustamante, P.; Cherel, Y. Identification of
635 Sources and Bioaccumulation Pathways of MeHg in Subantarctic Penguins : A Stable
636 Isotopic Investigation. *Sci. Rep.* **2018**, *8* (8865). [https://doi.org/10.1038/s41598-018-](https://doi.org/10.1038/s41598-018-27079-9)
637 *27079-9*.
- 638 (25) Point, D.; Sonke, J. E.; Day, R. D.; Roseneau, D. G.; Hobson, K. A.; Pol, S. S. Vander;
639 Moors, A. J.; Pugh, R. S.; Donard, O. F. X.; Becker, P. R. Methylmercury
640 Photodegradation Influenced by Sea-Ice Cover in Arctic Marine Ecosystems. *Nat. Geosci.*

- 641 **2011**, 4 (1), 1–7. <https://doi.org/10.1038/ngeo1049>.
- 642 (26) Day, R. D.; Roseneau, D. G.; Berail, S.; Hobson, K. a.; Donard, O. F. X.; Vander Pol, S.
643 S.; Pugh, R. S.; Moors, A. J.; Long, S. E.; Becker, P. R. Mercury Stable Isotopes in Seabird
644 Eggs Reflect a Gradient from Terrestrial Geogenic to Oceanic Mercury Reservoirs.
645 *Environ. Sci. Technol.* **2012**, 46 (10), 5327–5335. <https://doi.org/10.1021/es2047156>.
- 646 (27) Blum, J. D.; Sherman, L. S.; Johnson, M. W. Mercury Isotopes in Earth and Environmental
647 Sciences. *Annu. Rev. Earth Planet. Sci.* **2014**, 42, 249–269.
648 <https://doi.org/10.1146/annurev-earth-050212-124107>.
- 649 (28) Li, M.; Sherman, L. S.; Blum, J. D.; Grandjean, P.; Mikkelsen, B.; Weihe, P.; Sunderland,
650 E. M.; Shine, J. P. Assessing Sources of Human Methylmercury Exposure Using Stable
651 Mercury Isotopes. *Environ. Sci. Technol.* **2014**, 48 (15), 8800–8806.
652 <https://doi.org/10.1021/es500340r>.
- 653 (29) Cransveld, A. A. E.; Amouroux, D.; Tessier, E.; Koutrakis, E.; Ozturk, A. A.; Bettoso, N.;
654 Mieiro, C. L.; Berail, S.; Barre, J. P. G.; Sturaro, N.; Schnitzler, J. G.; Das, K. Mercury
655 Stable Isotopes Discriminate Different Populations of European Seabass and Trace
656 Potential Hg Sources around Europe. *Environ. Sci. Technol.* **2017**, 51 (21), 12219–12228.
657 <https://doi.org/10.1021/acs.est.7b01307>.
- 658 (30) Kritee, K.; Barkay, T.; Blum, J. D. Mass Dependent Stable Isotope Fractionation of
659 Mercury during Mer Mediated Microbial Degradation of Monomethylmercury. *Geochim.*
660 *Cosmochim. Acta* **2009**, 73 (5), 1285–1296. <https://doi.org/10.1016/j.gca.2008.11.038>.
- 661 (31) Kritee, K.; Blum, J. D.; Barkay, T. Mercury Stable Isotope Fractionation during Reduction
662 of Hg(II) by Different Microbial Pathways. *Environ. Sci. Technol.* **2008**, 42 (24), 9171–
663 9177. <https://doi.org/10.1021/es801591k>.
- 664 (32) Zheng, W.; Foucher, D.; Hintelmann, H. Mercury Isotope Fractionation during

- 665 Volatilization of Hg(0) from Solution into the Gas Phase. *J. Anal. At. Spectrom.* **2007**, 22
666 (9), 1097. <https://doi.org/10.1039/b705677j>.
- 667 (33) Kwon, S. Y.; Blum, J. D.; Chirby, M. a; Chesney, E. J. Application of Mercury Isotopes
668 for Tracing Trophic Transfer and Internal Distribution of Mercury in Marine Fish Feeding
669 Experiments. *Environ. Toxicol. Chem.* **2013**, 32 (10), 2322–2330.
670 <https://doi.org/10.1002/etc.2313>.
- 671 (34) Kwon, S. Y.; Blum, J. D.; Carvan, M. J.; Basu, N.; Head, J. A.; Madenjian, C. P.; David,
672 S. R. Absence of Fractionation of Mercury Isotopes during Trophic Transfer of
673 Methylmercury to Freshwater Fish in Captivity. *Environ. Sci. Technol.* **2012**, 46 (14),
674 7527–7534. <https://doi.org/10.1021/es300794q>.
- 675 (35) Masbou, J.; Point, D.; Sonke, J. E.; Frappart, F.; Perrot, V.; Amouroux, D.; Richard, P.;
676 Becker, P. R. Hg Stable Isotope Time Trend in Ringed Seals Registers Decreasing Sea Ice
677 Cover in the Alaskan Arctic. *Env. Sci Technol* **2015**, 49, 8977–8985.
678 <https://doi.org/10.1021/es5048446>.
- 679 (36) Chen, J.; Hintelmann, H.; Feng, X.; Dimock, B. Unusual Fractionation of Both Odd and
680 Even Mercury Isotopes in Precipitation from Peterborough, ON, Canada. *Geochim.*
681 *Cosmochim. Acta* **2012**, 90, 33–46. <https://doi.org/10.1016/j.gca.2012.05.005>.
- 682 (37) Gratz, L. E.; Keeler, G. J.; Blum, J. D.; Sherman, L. S. Isotopic Composition and
683 Fractionation of Mercury in Great Lakes Precipitation and Ambient Air. *Environ. Sci.*
684 *Technol.* **2010**, 44 (20), 7764–7770. <https://doi.org/10.1021/es100383w>.
- 685 (38) Sherman, L. S.; Blum, J. D.; Douglas, T. A.; Steffen, A. Frost Flowers Growing in the
686 Arctic Ocean-Atmosphere-Sea Ice-Snow Interface: 2. Mercury Exchange between the
687 Atmosphere, Snow, and Frost Flowers. *J. Geophys. Res. Atmos.* **2012**, 117 (3), 1–10.
688 <https://doi.org/10.1029/2011JD016186>.

- 689 (39) Demers, J. D.; Blum, J. D.; Zak, D. R. Mercury Isotopes in a Forested Ecosystem:
690 Implications for Air-Surface Exchange Dynamics and the Global Mercury Cycle. *Global*
691 *Biogeochem. Cycles* **2013**, *27* (1), 222–238. <https://doi.org/10.1002/gbc.20021>.
- 692 (40) Enrico, M.; Roux, G. Le; Maruszczak, N.; Heimbürger, L. E.; Claustres, A.; Fu, X.; Sun,
693 R.; Sonke, J. E. Atmospheric Mercury Transfer to Peat Bogs Dominated by Gaseous
694 Elemental Mercury Dry Deposition. *Environ. Sci. Technol.* **2016**, *50* (5), 2405–2412.
695 <https://doi.org/10.1021/acs.est.5b06058>.
- 696 (41) Keslinka, L. K.; Wojczulanis-Jakubas, K.; Jakubas, D.; Neubauer, G. Determinants of the
697 Little Auk (Alle Alle) Breeding Colony Location and Size in W and NW Coast of
698 Spitsbergen. *PLoS One* **2019**, *14* (3). <https://doi.org/10.1371/journal.pone.0212668>.
- 699 (42) Kovacs, K.; Lydersen, C. *Birds and Mammals of Svalbard. Tromsø: Norwegian Polar*
700 *Institute*; 2006.
- 701 (43) Harding, A. M. A.; Hobson, K. A.; Walkusz, W.; Dmoch, K.; Karnovsky, N. J.; Van Pelt,
702 T. I.; Lifjeld, J. T. Can Stable Isotope ($\Delta^{13}\text{C}$ and $\Delta^{15}\text{N}$) Measurements of Little Auk (Alle
703 Alle) Adults and Chicks Be Used to Track Changes in High-Arctic Marine Foodwebs?
704 *Polar Biol.* **2008**, *31* (6), 725–733. <https://doi.org/10.1007/s00300-008-0413-4>.
- 705 (44) Grémillet, D.; Welcker, J.; Karnovsky, N. J.; Walkusz, W.; Hall, M. E.; Fort, J.; Brown,
706 Z. W.; Speakman, J. R.; Harding, A. M. A. Little Auks Buffer the Impact of Current Arctic
707 Climate Change. *Mar. Ecol. Prog. Ser.* **2012**, *454*, 197–206.
708 <https://doi.org/10.3354/meps09590>.
- 709 (45) Fort, J.; Moe, B.; Strøm, H.; Grémillet, D.; Welcker, J.; Schultner, J.; Jerstad, K.;
710 Johansen, K. L.; Phillips, R. A.; Mosbech, A. Multicolony Tracking Reveals Potential
711 Threats to Little Auks Wintering in the North Atlantic from Marine Pollution and
712 Shrinking Sea Ice Cover. *Divers. Distrib.* **2013**, *19* (10), 1322–1332.

- 713 <https://doi.org/10.1111/ddi.12105>.
- 714 (46) Fort, J.; Gremillet, D.; Traisnel, G.; Amelineau, F.; Bustamante, P. Does Temporal
715 Variation of Mercury Levels in Arctic Seabirds Reflect Changes in Global Environmental
716 Contamination, or a Modification of Arctic Marine Food Web Functioning? *Environ.*
717 *Pollut.* **2016**, *211*, 382–388. <https://doi.org/10.1016/j.envpol.2015.12.061>.
- 718 (47) Furness, R. W.; Muirhead, S. J.; Woodburn, M. Using Bird Feathers to Measure Mercury
719 in the Environment: Relationships between Mercury Content and Moulting. *Mar. Pollut. Bull.*
720 **1986**, *17* (1), 27–30. [https://doi.org/10.1016/0025-326X\(86\)90801-5](https://doi.org/10.1016/0025-326X(86)90801-5).
- 721 (48) Honda, K.; Nasu, T.; Tatsukawa, R. Seasonal Changes in Mercury Accumulation in the
722 Black-Eared Kite, *Milvus Migrans Lineatus*. *Environ. Pollut. Ser. A, Ecol. Biol.* **1986**, *42*,
723 325–334. [https://doi.org/10.1016/0143-1471\(86\)90016-4](https://doi.org/10.1016/0143-1471(86)90016-4).
- 724 (49) Hobson, K. A.; Clark, R. G. Assessing Avian Diets Using Stable Isotopes I: Turnover of
725 ¹³C in Tissues. *Condor* **1992**, *94* (1), 181–188.
726 <https://doi.org/https://doi.org/10.2307/1368807>.
- 727 (50) Bearhop, S.; Waldron, S.; Votier, S. C.; Furness, R. W. Factors That Influence
728 Assimilation Rates and Fractionation of Nitrogen and Carbon Stable Isotopes in Avian
729 Blood and Feathers. *Physiol. Biochem. Zool.* **2002**, *75* (5).
730 <https://doi.org/https://doi.org/10.1086/342800>.
- 731 (51) Fort, J.; Beaugrand, G.; Gremillet, D.; Phillips, R. A. Biologging, Remotely-Sensed
732 Oceanography and the Continuous Plankton Recorder Reveal the Environmental
733 Determinants of a Seabird Wintering Hotspot. *PLoS One* **2012**, *7* (7).
734 <https://doi.org/10.1371/journal.pone.0041194>.
- 735 (52) Grissot, A.; Graham, I. M.; Quinn, L.; Bråthen, V. S.; Thompson, P. M. Breeding Status
736 Influences Timing but Not Duration of Moulting in the Northern Fulmar *Fulmarus Glacialis*.

- 737 *Ibis (Lond. 1859)*. **2019**, 1–14. <https://doi.org/10.1111/ibi.12714>.
- 738 (53) Carravieri, A.; Bustamante, P.; Churlaud, C.; Fromant, A.; Cherel, Y. Moulting Patterns
739 Drive Within-Individual Variations of Stable Isotopes and Mercury in Seabird Body
740 Feathers: Implications for Monitoring of the Marine Environment. *Mar. Biol.* **2014**, *161*,
741 963–968. <https://doi.org/10.1007/s00227-014-2394-x>.
- 742 (54) Peterson, S. H.; Ackerman, J. T.; Toney, M.; Herzog, M. P. Mercury Concentrations Vary
743 Within and Among Individual Bird Feathers: A Critical Evaluation and Guidelines for
744 Feather Use in Mercury Monitoring Programs. *Environ. Toxicol. Chem.* **2019**, *38* (6),
745 1164–1187. <https://doi.org/10.1002/etc.4430>.
- 746 (55) Renedo, M.; Bustamante, P.; Tessier, E.; Pedrero, Z.; Cherel, Y.; Amouroux, D.
747 Assessment of Mercury Speciation in Feathers Using Species-Specific Isotope Dilution
748 Analysis. *Talanta* **2017**, *174*, 100–110. <https://doi.org/10.1016/j.talanta.2017.05.081>.
- 749 (56) Renedo, M.; Amouroux, D.; Duval, B.; Carravieri, A.; Tessier, E.; Barre, J.; Bérail, S.;
750 Pedrero, Z.; Cherel, Y.; Bustamante, P. Seabird Tissues As Efficient Biomonitoring Tools
751 for Hg Isotopic Investigations: Implications of Using Blood and Feathers from Chicks and
752 Adults. *Environ. Sci. Technol.* **2018**, *52* (7), 4227–4234.
753 <https://doi.org/10.1021/acs.est.8b00422>.
- 754 (57) Yamakawa, A.; Takeuchi, A.; Shibata, Y.; Bérail, S.; Donard, O. F. X. Determination of
755 Hg Isotopic Compositions in Certified Reference Material NIES No. 13 Human Hair by
756 Cold Vapor Generation Multi-Collector Inductively Coupled Plasma Mass Spectrometry.
757 *Accredit. Qual. Assur.* **2016**, *21* (13), 197–202. [https://doi.org/10.1007/s00769-016-1196-](https://doi.org/10.1007/s00769-016-1196-x)
758 [x](https://doi.org/10.1007/s00769-016-1196-x).
- 759 (58) R Core Team, 2016: A Language and Environment for Statistical Computing. R
760 Foundation for Statistical Computing, Vienna, Austria.

- 761 (59) Bates, D.; Mächler, M.; Bolker, B. M.; Walker, S. C. Fitting Linear Mixed-Effects Models
762 Using Lme4. *J. Stat. Softw.* **2015**, *67* (1). <https://doi.org/10.18637/jss.v067.i01>.
- 763 (60) Salmerón, R.; García, C. B.; García, J. Variance Inflation Factor and Condition Number
764 in Multiple Linear Regression. *J. Stat. Comput. Simul.* **2018**, *88* (12), 2365–2384.
765 <https://doi.org/https://doi.org/10.1080/00949655.2018.1463376>.
- 766 (61) Zuur, A. F.; Ieno, E. N.; Walker, N. J.; Saveliev, A. A.; Smith, G. M. Mixed Effects
767 Models and Extensions in Ecology with R. *J. Stat. Softw.* **2009**, *32* (Book Review 1), 1–
768 4. <https://doi.org/10.18637/jss.v032.b01>.
- 769 (62) Meredith, M. M. Package ‘Wiqid.’ **2020**.
- 770 (63) Jaeger, B. C. Computes R Squared for Mixed (Multilevel) Model. *Packag. ‘r2glmm’* **2017**,
771 12.
- 772 (64) Davis, W. C.; Vander Pol, S. S.; Schantz, M. M.; Long, S. E.; Day, R. D.; Christopher, S.
773 J. An Accurate and Sensitive Method for the Determination of Methylmercury in
774 Biological Specimens Using GC-ICP-MS with Solid Phase Microextraction. *J. Anal. At.*
775 *Spectrom.* **2004**, *19* (12), 1546–1551. <https://doi.org/10.1039/b412668h>.
- 776 (65) Bond, A. L.; Diamond, A. W. Total and Methyl Mercury Concentrations in Seabird
777 Feathers and Eggs. *Arch. Environ. Contam. Toxicol* **2009**, 286–291.
778 <https://doi.org/10.1007/s00244-008-9185-7>.
- 779 (66) Rosing-Asvid, A.; Hedeholm, R.; Arendt, K. E.; Fort, J.; Robertson, G. J. Winter Diet of
780 the Little Auk (*Alle Alle*) in the Northwest Atlantic. *Polar Biol.* **2013**, *36* (11), 1601–1608.
781 <https://doi.org/10.1007/s00300-013-1379-4>.
- 782 (67) Fort, J.; Cherel, Y.; Harding, A. M. A.; Welcker, J.; Jakubas, D.; Steen, H.; Karnovsky,
783 N. J.; Grémillet, D. Geographic and Seasonal Variability in the Isotopic Niche of Little
784 Auks. *Mar. Ecol. Prog. Ser.* **2010**, *414*, 293–302. <https://doi.org/10.3354/meps08721>.

- 785 (68) Welcker, J.; Harding, A. M. A.; Karnovsky, N. J.; Steen, H.; Strøm, H.; Gabrielsen, G. W.
786 Flexibility in the Bimodal Foraging Strategy of a High Arctic Alcid, the Little Auk Alle
787 Alle. *J. Avian Biol.* **2009**, *40* (4), 388–399. [https://doi.org/10.1111/j.1600-](https://doi.org/10.1111/j.1600-048X.2008.04620.x)
788 [048X.2008.04620.x](https://doi.org/10.1111/j.1600-048X.2008.04620.x).
- 789 (69) Hobson, K. A.; Clark, R. G. Assessing Avian Diets Using Stable Isotopes II: Factors
790 Influencing Diet-Tissue Fractionation. *Condor* **1992**, *94* (1), 189–197.
791 [https://doi.org/https://doi.org/10.2307/1368808](https://doi.org/10.2307/1368808).
- 792 (70) Graham, B. S.; Koch, P. L.; Newsome, S. D.; McMahon, K. W.; Aurioles, D. Using
793 Isoscapes to Trace the Movements and Foraging Behavior of Top Predators in Oceanic
794 Ecosystems. In *Isoscapes: Understanding Movement, Pattern, and Process on Earth*
795 *Through Isotope Mapping*; 2010; pp 299–318. [https://doi.org/https://doi.org/10.1007/978-](https://doi.org/10.1007/978-90-481-3354-3_14)
796 [90-481-3354-3_14](https://doi.org/10.1007/978-90-481-3354-3_14).
- 797 (71) McMahon, K. W.; Hamady, L. L.; Thorrold, S. R. A Review of Ecogeochemistry
798 Approaches to Estimating Movements of Marine Animals. *Limnol. Oceanogr.* **2013**, *58*
799 (2), 697–714. <https://doi.org/10.4319/lo.2013.58.2.0697>.
- 800 (72) Kürten, B.; Painting, S. J.; Struck, U.; Polunin, N. V. C.; Middelburg, J. J. Tracking
801 Seasonal Changes in North Sea Zooplankton Trophic Dynamics Using Stable Isotopes.
802 *Biogeochemistry* **2013**, *113* (1–3), 167–187. <https://doi.org/10.1007/s10533-011-9630-y>.
- 803 (73) Renedo, M.; Pedrero, Z.; Amouroux, D.; Cherel, Y.; Bustamante, P. Mercury Isotopes of
804 Key Tissues Document Mercury Metabolic Processes in Seabirds. *Chemosphere* **2020**,
805 *127777*. <https://doi.org/10.1016/j.chemosphere.2020.127777>.
- 806 (74) Stempniewicz, L.; Skakuj, M.; Iliszko, L. The Little Auk Alle Alle Polaris of Franz Josef
807 Land: A Comparison with Svalbard Alle a. Alle Populations. *Polar Res.* **1996**, *15* (1), 1–
808 10. <https://doi.org/10.3402/polar.v15i1.6632>.

- 809 (75) Motta, L. C.; Blum, J. D.; Johnson, M. W.; Umhau, B. P.; Popp, B. N.; Washburn, S. J.;
810 Drazen, J. C.; Benitez-Nelson, C. R.; Hannides, C. C. S.; Close, H. G.; Lamborg, C. H.
811 Mercury Cycling in the North Pacific Subtropical Gyre as Revealed by Mercury Stable
812 Isotope Ratios. *Global Biogeochem. Cycles* **2019**, *33* (6), 777–794.
813 <https://doi.org/10.1029/2018GB006057>.
- 814 (76) Burt, A.; Wang, F.; Pučko, M.; Mundy, C. J.; Gosselin, M.; Philippe, B.; Poulin, M.;
815 Tremblay, J. É.; Stern, G. A. Mercury Uptake within an Ice Algal Community during the
816 Spring Bloom in First-Year Arctic Sea Ice. *J. Geophys. Res. Ocean.* **2013**, *118* (9), 4746–
817 4754. <https://doi.org/10.1002/jgrc.20380>.
- 818 (77) Schartup, A. T.; Balcom, P. H.; Soerensen, A. L.; Gosnell, K. J.; Calder, R. S. D.; Mason,
819 R. P.; Sunderland, E. M. Freshwater Discharges Drive High Levels of Methylmercury in
820 Arctic Marine Biota. *Proc. Natl. Acad. Sci.* **2015**, *112* (38), 11789–11794.
821 <https://doi.org/10.1073/pnas.1505541112>.
- 822 (78) Renedo, M.; Bustamante, P.; Cherel, Y.; Pedrero, Z.; Tessier, E.; Amouroux, D. A
823 “Seabird-Eye” on Mercury Stable Isotopes and Cycling in the Southern Ocean. *Sci. Total*
824 *Environ.* **2020**, *742*, 140499. <https://doi.org/10.1016/j.scitotenv.2020.140499>.
- 825 (79) Masbou, J.; Sonke, J. E.; Amouroux, D.; Guillou, G.; Becker, P. R.; Point, D. Hg-Stable
826 Isotope Variations in Marine Top Predators of the Western Arctic Ocean. *ACS Earth Sp.*
827 *Chem.* **2018**, *2* (0), 479–490. <https://doi.org/10.1021/acsearthspacechem.8b00017>.
- 828 (80) Lynch-Stieglitz, J.; Stocker, T. F.; Broecker, W. S.; Fairbanks, R. G. The Influence of Air-
829 sea Exchange on the Isotopic Composition of Oceanic Carbon: Observations and
830 Modeling. *Global Biogeochem. Cycles* **1995**, *9* (4), 653–665.
831 <https://doi.org/https://doi.org/10.1029/95GB02574>.
- 832 (81) Gruber, N.; Keeling, D.; Bacastow, R. B.; Guenther, P. R.; Lueker, T. J.; Wahlen, M.;

- 833 Meijer, H. a J.; Mook, W. G.; Stocker, T. F. Spatiotemporal Patterns of Carbon-13 in the
834 Global Surface Oceans and the Oceanic Suess Effect. *Global Biogeochem. Cycles* **1999**,
835 *13* (2), 307–335. <https://doi.org/10.1029/1999GB900019>.
- 836 (82) Fontela, M.; García-Ibáñez, M. I.; Hansell, D. A.; Mercier, H.; Pérez, F. F. Dissolved
837 Organic Carbon in the North Atlantic Meridional Overturning Circulation. *Sci. Rep.* **2016**,
838 *6*, 1–9. <https://doi.org/10.1038/srep26931>.
- 839 (83) Li, M.; Schartup, A. T.; Valberg, A. P.; Ewald, J. D.; David, P.; Yin, R.; Balcom, P. H.;
840 Sunderland, E. M. Environmental Origins of Methylmercury Accumulated in Subarctic
841 Estuarine Fish Indicated by Mercury Stable Isotopes. *Env. Sci Technol* **2016**, *50*, 11559–
842 15568. <https://doi.org/10.1021/acs.est.6b03206>.
- 843